The Evaluation of MEOSS Airborne Three-Line Scanner Imagery: Processing Chain and Results

C. Heipke, W. Kornus, and A. Pfannenstein

Abstract

A completely digital processing chain realized for the evaluation of airborne three-line scanner imagery acquired by the Monocular Electro-Optical Stereo Scanner (MEOSS) is described. It involves image matching, photogrammetric point determination, and the generation of a digital terrain model (DTM). The computations were carried out using image data from one flight path and from two crossing paths, with and without navigation data as additional observations for the exterior orientation parameters.

The derived results were checked using independent measurements from medium-scale aerial frame imagery. Empirical standard deviations of about 1 m (0.5 pixel) in X and Y, respectively, and 2.0 m (1 pixel) in height were obtained for the crossing flight paths. Whereas the navigation data turned out to be essential for the processing of one flight path, they were not necessary for the simultaneous processing of both paths. Subsequently, a DTM was derived from up to six rays per object point, thus reducing the effect of gross errors inherent in image matching. The DTM represents the visible Earth's surface, including houses, vegetation, etc., rather than being a "bare earth DTM," which is usually derived from interactive measurements. These results demonstrate the usefulness and applicability of airborne three-line scanner imagery for photogrammetry.

Introduction

With the introduction of digital techniques in the last decades, revolutionary changes have occurred in photogrammetry. Examples are the successful use of digital orthoprojection and of automatic image matching procedures. Data acquisition, however, largely relies on film-based frame cameras, because CCD arrays with a comparable size and resolution are not available, and are not likely to be available in the near future. In order to exploit the advantages of digital processing, the film images have to be scanned in a separate step, which is time and cost consuming and may introduce additional errors.

With these developments in mind, high resolution CCD line sensors are an interesting alternative for aerial and even more so for space photogrammetry. They offer the advantage of direct digital image acquisition, but require more sophisticated processing techniques, because the imagery is taken while the sensor is moving. For mapping from space, the French Satellite SPOT (pour l'observation de la terre), equipped with a single CCD line sensor, successfully illustrates this concept. Stereo images are acquired in successive orbit paths. More rigorous processing, however, requires three-line scanner imagery. In this case, stereo images are recorded quasi simultaneously and the geometric properties of the imagery are much more favorable. For airborne images, the movement variations of the sensor carrier (the aircraft) during image acquisition are much larger than for space applications and constitute an additional challenge.

The importance of three-line scanners is also reflected in the funding of the three-line scanner space projects MOMS-02/D2 (Ackermann *et al.*, 1989) and Mars 94-HRSC/WAOSS (Neukum and Tarnopolski, 1990; Oertel *et al.*, 1992; Albertz *et al.*, 1993) by the German Space Agency (DARA). Both projects are being carried out under the supervision of the German Aerospace Research Establishment (DLR). The Chair for Photogrammetry and Remote Sensing, Technical University Munich, is involved in both projects. A common major objective is the realization of and the software development for a completely digital photogrammetric processing chain for spaceborne three-line scanner imagery from data acquisition to the generation of DTM and orthoimage maps.

The Modular Optoelectronic Multispectral Scanner (MOMS-02/D2) is an Earth observation experiment in the course of the second German spacelab mission D2, and was successfully flown in spring 1993. MOMS-02 consists of five lenses for simultaneous high resolution, stereo, and multispectral data acquisition. The stereo module consists of three lenses with one CCD sensor line each, which provide a forward-, a nadir- and a backward-looking view. The central lens enables high quality data acquisition with a ground resolution of 4.5 m/pixel. The other two lenses allow for a recording of multispectral information. The first promising results of photogrammetric processing of MOMS-02/D2 data have been reported recently (Lehner and Kornus, 1994).

Two multi-line scanners, the High Resolution Stereo Camera (HRSC) and the Wide Angle Optoelectronic Stereo Scanner (WAOSS) will fly to planet Mars on board a Russian orbiter scheduled for launch in the fall of 1994. The HRSC consists of nine CCD sensor lines, which acquire high resolution stereo (up to 10 m/pixel) and multispectral imagery of the Martian surface. The WAOSS consists of three CCD sensor lines for stereo data acquisition in the moderate (up to 80 m/pixel) and low resolution (1,000 m/pixel) range. The HRSC will provide accurate information for selected areas, whereas a complete coverage of Mars will be obtained from WAOSS imagery. The WAOSS has been flown on board an aircraft (Reulke *et al.*, 1992). These tests were designed for improving the scanner itself; the recorded imagery is not well suited for photogrammetric processing.

In addition to the MOMS-02/D2 and Mars 94-HRSC/WAOSS, two further three-line scanners have been developed in Germany. The Monocular Electro-Optical Stereo Scanner (MEOSS) (Lanzl, 1986) was built under the management of the

Lehrstuhl für Photogrammetrie und Fernerkundung, Technische Universität München, Arcisstrasse 21, D-80333 München, Germany.

Photogrammetric Engineering & Remote Sensing, Vol. 62, No. 3, March 1996, pp. 293–299.

0099-1112/96/6203–293$3.00/0

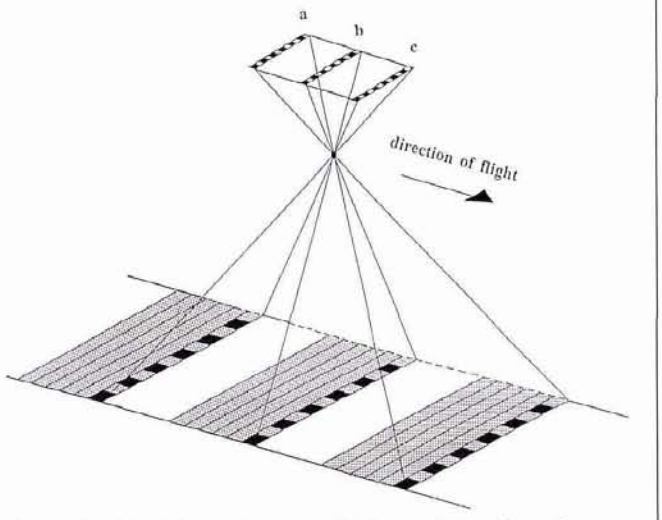

Figure 1. Principle of data acquisition using a three-line scanner.

DLR. After some airborne test flights, MEOSS was to circle the Earth on an Indian satellite. Unfortunately, the camera was lost in a launch failure in fall 1993. The airborne Digitales Photogrammetrisches Auswertesystem (DPA) scanner (Hofmann, 1986), financed by the German military, has been recently tested with promising results (Hofmann *et al.*, 1993).

Until the release of the MOMS-02/D2 imagery, the only three-line scanner data available to the civilian photogrammetric community were those from the airborne test flights with MEOSS. The analysis of the results of the first flight in June 1986 (Lehner and Gill, 1989; Kornus, 1989; Heipke *et al.*, 1990) pointed out a number of necessary improvements and led to a refined second flight three years later. This paper contains the results of the imagery from the two flight paths of the second flight. An analysis of the same image material using only one flight path is given by Lehner and Gill (1992).

The principle of image data acquisition using three-line scanners is depicted in Figure 1. The parameters of exterior orientation are estimated by means of a photogrammetric bundle adjustment based on extended collinearity equations. These parameters are determined only at certain time intervals for so-called orientation images. Between these intervals, the temporal course of the parameters is modeled by a suitable function. For a further description of the functional model, see Hofmann *et al.* (1982), Müller (1991), and Ebner *et al.* (1992). The three-line geometry is characterized by parallel projection in the flight direction and central perspective projection perpendicular to the flight direction. Simulation studies (Ebner *et al.*, 1991; 1992) have shown that, due to the parallel projection, navigation data have to be introduced as additional observations for the exterior orientation parameters into the bundle adjustment in order to achieve satisfactory results, if only one flight path with three image strips is available. If image data from two crossing flight paths (six image strips) are used, the influence of the additional observations is a lot less pronounced.

These findings were to be verified with practical data in this study. The computations were carried out for four different cases: using one flight path with and without navigation data, and using both flight paths simultaneously, again with and without navigation data. Additionally, a DTM was derived in an area of five- and sixfold overlap. Due to the fact that up to six rays per object point contributed to the DTM, matching errors could be detected to a large extent. The resulting DTM describes the visible surface of the Earth, including houses, vegetation, etc.

Data Processing and Results

Input Data and Processing Flow

In this section we describe a completely digital processing chain realized for the evaluation of airborne three-line scanner imagery acquired by MEOSS. The imagery was taken in June 1989 and depicts a rural area near Dorfen, about 40 km to the East of Munich in Germany. The processing involves image matching, photogrammetric point determination, and the generation of a digital terrain model (DTM). The MEOSS parameters are listed in Table 1.

The following input data were available:

- Image Data: Six image strips, three from the north/south (NS) flight path and three from the west/east (WE) flight path, respectively, with a five- and sixfold overlapping area (see Figure 2). The image data were radiometrically preprocessed at the DLR.
- Navigation Data: *XYZ* positions from the aircraft navigation system for every 40th scan line with a resolution of a few centimetres. Roll, pitch, and yaw angles from an inertial navigation system (INS) for every fourth image line with a resolution of 0.005°. Accuracy figures for both sets of observations were not available.
- Geometric System Calibration Data: Angle measurements to 17 pixels per CCD array with an accuracy better than 0.5 pixel.
- Two analog aerial frame images of scale 1:15,000 (c = 153 mm) with an overlap of approximately 70 perecent, taken in 1988.
- Ground coordinates of 57 object points with a standard deviation of 0.33 m in X and Y and 0.48 m in Z, all located in the five- and sixfold overlapping area of the MEOSS image strips.
- A DTM in an area of 2.5 km by 3.5 km with a grid spacing of 10 m, generated using the DTM software package HIFI (Ebner *et al.*, 1988). The input data for HIFI were about 11,000 single points and 3,000 additional break line points measured interactively in the frame images (see Figure 2).

The processing flow is shown in Figure 3. Image coordinates of the 57 object points, mentioned above, were interactively measured in mono in all five or six MEOSS image strips. Using this information, image matching was performed. The available system calibration data were transformed into interior orientation parameters, a suitable distance between the orientation images was derived from the INS data, and, subsequently, a bundle adjustment was performed using a geometrically well distributed subset of the corresponding points. Finally, a DTM was generated from all corresponding points transformed into object space by employing a multiple forward intersection. The derived results were checked using the reference data. The above processing flow is described in detail in the following sections.

TABLE 1. MEOSS SENSOR AND IMAGING PARAMETERS

Nominal focal length	61.1 mm
Number of pixels per array	3236
Field of view	32°
Instantaneous field of view	0.01°
Scan line frequency	92.978 Hz
Mean flying height	11,335 m
Image scale	1 : 180,000
Ground pixel resolution	2.0 m by 2.0 m
Length of NS flight path	16.8 km (8416 rows)
Swath of NS flight path	6.4 km (3236 rows)
Length of WE flight path	16.9 km (8437 rows)
Swath of WE flight path	6.4 km (3236 rows)

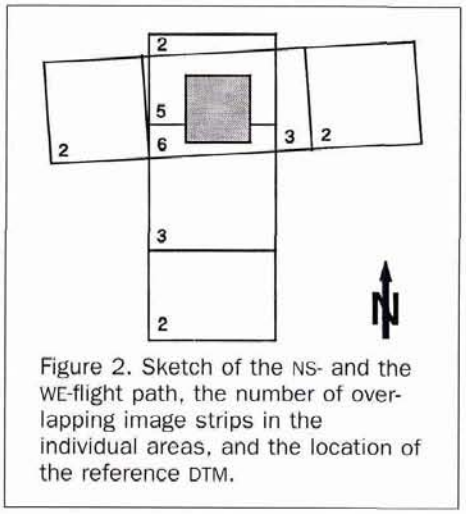

Figure 2. Sketch of the NS- and the WE-flight path, the number of overlapping image strips in the individual areas, and the location of the reference DTM.

Digital Image Matching

Least-squares image matching (Förstner, 1982; Heipke, 1990) is known to yield the most accurate results of all matching algorithms in the presence of adequate texture. This method has also been applied to satellite imagery (Otto and Chau, 1989). Their region growing algorithm, working on two images at a time, has been refined with respect to robustness of the results and has been successfully used in various projects (Heipke and Kornus, 1991; Heipke *et al.*, 1994). It was further improved for this study in order to match the six overlapping image strips.

In the following, a short explanation of the region-growing matching algorithm is given (for more details, refer to Otto and Chau (1989) and Heipke and Kornus (1991)). In order to simplify the explanation, we start with only two images. One pair of corresponding points is assumed to be approximately known. It is called the starting point. Normally, image coordinates of GCPs are used as starting points, because they have to be measured interactively anyway. Least-squares image matching is carried out using the two matrices surrounding the starting point in both images. Thus, for the point in the left image remaining unchanged, the exact coordinates of the corresponding point in the right image are computed, as well as the correlation coefficient between the two matrices. Next, both matrices are shifted by a constant amount to the left (this amount is called STEP in the following) and the matching is repeated in the new position. The same is done for the positions to the right, on top, and under the starting point. The results for all four neighbors of the starting point are entered in a list in the order of decreasing value of the correlation coefficient.

The first point of this list is chosen as the new starting point. All its remaining neighbors in the distance of STEP are matched and, if the correlation coefficient lies above a certain threshold, the results are entered in the list. If more than one starting point is available, all of them are matched as described and the results are entered in the list. In this way, the whole overlapping area of the two images is processed, producing a regularly spaced grid of points in the left image and a deformed grid of corresponding points in the right image.

For all matching runs, the size of the template matrix was set to 15 by 15 pixels. A value of 9 pixels was used for STEP, and the threshold for the correlation coefficient was chosen to be 0.7. First the NS-nadir looking strip (which was considered as the left image in all runs) was matched with the NS-forward looking strip, then with the NS-backward looking strip, and, subsequently, with the WE-nadir looking strip. The same starting points were used in all three runs, and therefore the same positions in the NS-nadir looking strip were used, yielding corresponding points in all four strips.

The WE-nadir looking strip (now considered the left image) was then matched with the WE-forward looking strip and finally with the WE-backward looking strip. In these two runs, rather than using a regular grid of points in the nadir looking strip, points obtained from the NS-nadir/WE-nadir matching in the vicinity of the regular grid points were used if available. Thus, corresponding points in all six strips were generated.

Altogether, about 500,000 pairs of corresponding points corresponding to 2,000,000 image coordinates were derived in the five matching runs. From this large number, a subset of 123,316 image coordinates of geometrically well distributed points was selected for introduction into the bundle adjustment. The selection criterium was a local maximum of the correlation coefficient. Although a number of plausibility checks was carried out within the matching runs, this subset still contained a number of gross errors due to inherent problems of image matching (repetitive patterns, low texture, etc).

Preprocessing of the Calibration Data

The geometry of a three-line scanner is somewhat different from that of a frame camera. For optimum focusing, the CCD arrays are not located in a common image plane, but are slightly displaced in the *z*-direction. The geometry of MEOSS

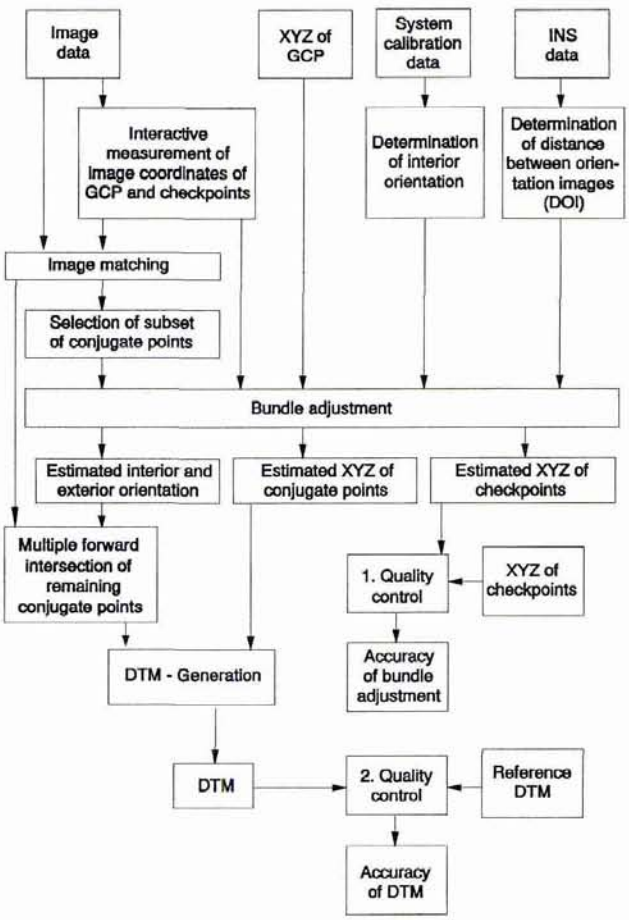

Figure 3. MEOSS processing data flow.

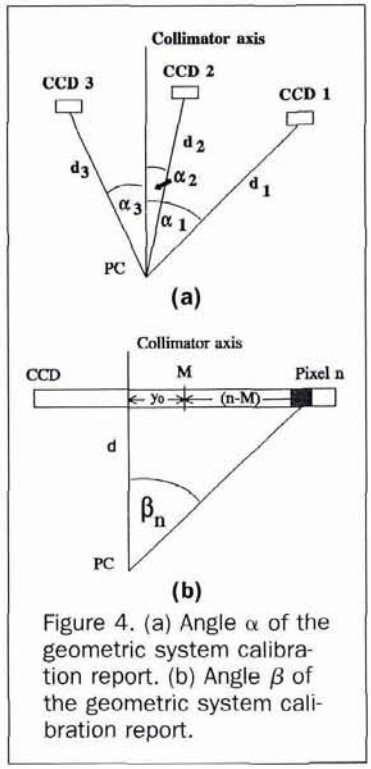

Figure 4. (a) Angle α of the geometric system calibration report. (b) Angle β of the geometric system calibration report.

is described by the results of a geometric system calibration, which was performed at the DLR using goniometer equipment. For 17 elements of each CCD array (200-pixel spacing), two image angles α and β were measured with reference to the collimator axis. Figures 4a and 4b show the measurement setup in two vertical sections, perpendicular to each other. In the zero-position ($\alpha = \beta = 0$), the collimator axis was assumed to be aligned parallel to the optical axis of the MEOSS lens. The mathematical projection center, PC, was defined as the axial intercept of the two goniometer axes. In order to approximate this geometry, a model based on nine parameters, three parameters for each of the three CCD arrays, was developed:

- convergence angle: α_1, α_2, α_3;
- distance between the CCD array and the PC: d_1, d_2, d_3; and
- displacement of the collimator axis from the center of the CCD array in line direction: y_{01}, y_{02}, y_{03}.

For each CCD array, these parameters were derived from the corresponding image angles by a least-squares adjustment. Assuming a constant pixel size $P_x = 10.7$ µm, the observation equations for each calibrated pixel in each CCD array read

$$v_\alpha = \hat{\alpha} - \alpha$$

$$v_\beta = a\tan\frac{\hat{y}_0 + (n-M)\,p_x}{\hat{d}} - \beta$$

where M is the center of the CCD array (i.e., 3236/2 + 0.5 = 1618.5) and n the column of the calibrated pixel (other symbols are explained in the text).

The results of the adjustment are listed in Table 2. Deviations from the introduced model, caused, for example, by sensor deformation and lens distortion, were calculated for each calibrated pixel from the residuals of the adjustment (see Figure 5). Displacements for the center of each single sensor element in the row and column directions were interpolated from these deviations using a third-order polynomial. Subsequently, corrections for all image coordinates obtained from interactive measurement and image matching (see previous sections) were derived by linear interpolation between the two neighboring pixel centers.

Determination of the Distance between the Orientation Images

The distance between the orientation images (DOI) is of high concern for the reconstruction of the exterior orientation. It must be chosen short enough to sufficiently approximate the temporal course of all six orientation parameters. A DOI too large means that this approximation is too inaccurate, leading to systematic model errors. A DOI too short increases the number of unknowns in the bundle adjustment and, thus, decreases the stability of the photogrammetric block.

The DOI was derived by analyzing the given INS measurements. In order to obtain an estimate of the model errors, the residuals of the INS measurements derived from adjusting third-order polynomials using different DOI (expressed in image rows) were calculated. The corresponding root-mean-square (RMS) values are listed in Table 3.

A DOI of 80 rows introduces a mean interpolation error of 0.017 degrees or 1.7 pixels for the pitch angle. For a DOI of 40 rows, all three RMS values lie below 0.01 degree and are not significantly reduced by an even shorter DOI. Based on these results, a DOI of 40 rows was chosen, corresponding to a flight distance of 80 m and a flight time of 0.42 seconds.

Bundle Block Adjustment

The bundle block adjustment requires different sets of input information, whose derivation was described in the previous chapters:

- image coordinates of corresponding points, GCPs, and check points;
- ground coordinates of the GCPs;
- parameters of the interior orientation; and
- optionally, additional control information (e.g., navigation data).

In order to study the influence of the navigation data on the bundle adjustment, results four different versions were computed:

- Version A: Simultaneous adjustment of the two flight paths, *including navigation data*;
- Version B: Simultaneous adjustment of the two flight paths, excluding navigation data;
- Version C: Single path adjustment of the W/E path, including navigation data; and
- Version D: Single path adjustment of the W/E path, excluding navigation data.

The following data were introduced as observations (see also Figure 2; values in brackets are valid for Versions C and D):

- Six-hundred two (342) image coordinates of 12 GCPs and 45 check points in the five- and sixfold overlap area measured interactively with a standard deviation of 4 µm (approximately 0.4 pixel);
- One-hundred four thousand, nine-hundred fifty (57,146) of the 123,316 image coordinates derived from image matching with a standard deviation of 2.7 µm (approximately 0.25 pixel). 18,366 image coordinates were recognized as gross errors and eliminated in three preliminary bundle adjustment runs. A threshold for the residuals was used as the criterium for the elimination. The remaining corresponding points are

TABLE 2. INTERIOR ORIENTATION PARAMETERS OF MEOSS

	CCD 1 (backward)	CCD 2 (nadir)	CCD 3 (forward)
$\hat{d}$ [mm]	67.067 ± 0.008	61.623 ± 0.005	67.072 ± 0.011
$\hat{\alpha}$ [deg]	−23.488 ± 0.001	0.035 ± 0.001	23.563 ± 0.002
$\hat{y}_0$ [µm]	69.8 ± 1.2	67.4 ± 0.7	71.4 ± 1.7

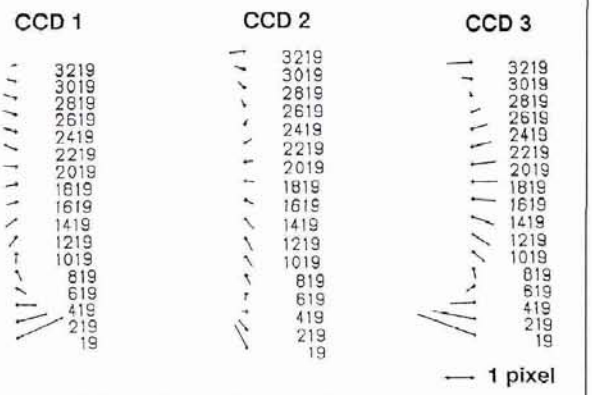

Figure 5. Deviations of the calibrated pixel centers from the model.

still geometrically well distributed. Gross error detection was only carried out for version B. The 57,146 observations for versions C and D were subsequently derived from the cleaned data set;

- Thirty-six ground coordinates of the 12 GCPs with a standard deviation of 0.33 m in X and Y and 0.48 m in Z. Although seven GCP coordinates are sufficient in principle, four groups of three GCPs, each located in the corners of the overlapping area, were used to ensure a precise definition of the datum for the follow-on quality control;
- Nine parameters of the interior orientation (for the introduced standard deviations, see Table 2); and
- Navigation data, i.e., additional observations for 2,538 (1,272) exterior orientation parameters at the times of the 423 (212) orientation images with standard deviations of $\sigma_{X_0} = \sigma_{Y_0} =$ 100 m, $\sigma_{Z_0} = 20$ m, $\sigma_\varphi = \sigma_\omega = \sigma_\kappa = 0.045$ degrees. Although these standard deviations could not be verified from the measurements, they should not be too optimistic (Versions A and C only).

From these observations, the following unknowns were estimated:

- Forty-seven thousand, three-hundred ninety-seven (33,549) ground coordinates of 15,799 (11,183) object points, including the 12 GCPs and 45 check points;
- Two-thousand, five-hundred thirty-eight (1,272) parameters of exterior orientation for a total of 423 (212) orientation images in both paths;
- Nine parameters of interior orientation; and
- Eighteen (nine) additional unknowns in order to model systematic errors of the navigation data.

Table 4 contains the RMS values of the empirical and the theoretical standard deviations for all 45 check points. The theoretical values are derived from the inverted normal equation matrix and the *a posteriori* σ_0 value of the bundle adjustment. The empirical values are derived by comparing the estimated ground coordinates of the check points against the known values.

The empirical standard deviations of Version B show that accuracies of about 1 m (0.5 pixel) in X and Y, respectively, and 2.0 m (1 pixel) in height were obtained. These results are in accordance with evaluations of other airborne three-line scanner imagery (Hofmann *et al.*, 1993) and demonstrate the potential of this concept. In order to prove that point determination is also possible with minimum control information, additional adjustment runs using seven GCP coordinates (two XYZ GCPs and one Z GCP) instead of 36 were executed. In this case, no redundancy exists in the definition of the datum, and errors in the GCP coordinates lead to systematically incorrect object coordinates. In these examples the resulting deterioration of the empirical accuracies was in the range of 10 percent and 20 percent.

The good correspondence between the theoretical and the empirical standard deviations demonstrates the feasibility of photogrammetric point determination of airborne three-line scanner imagery. Comparing Versions A and B as well as C and D, the influence of navigation data becomes evident. The use of navigation data considerably improves the accuracy of the single-path adjustment, especially in X and in Z. For the W/E path, the X-axis points approximately in the flight direction. Because three-line scanner imagery provides a parallel projection in, and a central perspective projection only perpendicular to, the flight direction, the component in the flight direction and the height can only be determined with lower accuracy as compared to the component perpendicular to the flight direction. Therefore, in this example the Y coordinates are determined much more accurately than the X and Z coordinates in Version D. By introducing the navigation data, this disadvantage can only partly be compensated for (see the results of Version C).

The results of Versions A and B show that this basic weakness of the line scanner geometry is completely overcome if two crossing flight paths are involved. In the overlap area, a CCD sensor line of one path can tie together various lines of the other path and vice versa. In this way, the geometrically weak parallel projection is stabilized. The high geometric stability of this configuration has already been demonstrated by computer simulations (Ebner *et al.*, 1992), and is proven in a practical test for the first time in this paper. The results of Versions A and B show that the simultaneous adjustment of two crossing strips leads to a significantly improved accuracy compared to a single strip adjustment. In this case, it is possible to ignore the navigation data because they have no significant effect on the results. Further computations are therefore conducted for the results of Version B only.

Table 4 reflects the empirical accuracy of the interactively measured points. In order to obtain an accuracy estimate also for the automatically derived tie points, the heights of 395 points randomly distributed in the five- and six-fold overlap area were derived interactively in the aerial frame images by prepositioning at the adjusted XY coordinates and then measuring Z. A subset of 251 points was selected lying on the earth surface and excluding points, e.g., on top of trees or houses. The RMS value of the differences between the measured and the adjusted heights resulted in an empirical standard deviation of 2.4 m, which also matches the corresponding theoretical value of 2.0 m well.

Generation of a Digital Terrain Model

A DTM represents a very important product of photogrammetry. It is essential for any spatial analysis which needs the third dimension as input, and, therefore, it is increasingly being incorporated into geographic information systems (GIS). Furthermore, the DTM serves as input information for computing an orthoimage which, apart from the value in itself, constitutes another data source for GIS. Thus, the quality of the resulting DTM is important for assessing the concept of three-line scanners.

Using the exterior orientation parameters derived in the bundle adjustment as constant values, the corresponding

TABLE 3. RMS VALUES OF THE RESIDUALS OF THE NAVIGATION DATA DERIVED FROM ADJUSTING THIRD-ORDER POLYNOMIALS (0.01° IS EQUIVALENT TO 1 PIXEL FOR ROLL AND PITCH)

	DOI = 20 rows	DOI = 40 rows	DOI = 80 rows
Roll angle	0.003°	0.003°	0.008°
Pitch angle	0.005°	0.006°	0.017°
Yaw angle	0.003°	0.004°	0.006°

TABLE 4. RMS VALUES OF THE THEORETICAL AND EMPIRICAL STANDARD DEVIATIONS DERIVED FROM 45 CHECK POINTS.

	Theoretical Standard Deviations				Empirical Standard Deviations			
MEOSS	A	B	C	D	A	B	C	D
X [m]	1.0	1.0	5.7	7.0	1.1	1.1	8.9	12.5
Y [m]	1.0	1.0	1.4	1.7	0.9	0.9	1.4	1.8
Z [m]	3.1	3.2	4.3	5.2	2.0	2.0	3.4	5.8

points from image matching were transformed into object space by overdetermined multiple forward intersection of up to six image rays. Points with high residuals, pointing to gross matching errors, were identified and eliminated. In this way, the object points could be determined very robustly. About 11,000 of them lie in the area covered by the reference DTM. These 11,000 object points were used to create a DTM, called MEOSS-DTM, with a grid size of 10 m. Also, this MEOSS-DTM must be considered nearly free of matching errors due to the mentioned robustness of the input points for the DTM. It must be said, however, that, because distinct geomorphological features are not incorporated into the concept of matching and DTM generation, the MEOSS-DTM may be erroneous near breaklines, single points, etc. Another precondition for a correct DTM is adequate image texture, and, thus, a dense geometric distribution of corresponding points. In this study, no problems with low texture occurred.

The reference and the MEOSS-DTM are shown in Figure 6. Figure 7 shows the difference DTM. The same perspective as in Figure 6 was used. Comparing both DTMs, one has to take into account that they describe different object surfaces. An operator interactively collecting input data for a DTM usually tries to measure on the Earth surface itself, e.g., not on top of trees or houses. Accordingly, the reference DTM is defined as a so-called "bare Earth" DTM. A DTM derived by image matching, on the other hand, represents the visible surface, including all natural objects (vegetation) and man-made constructions (houses, etc.). Thus, the surface of the MEOSS-DTM should lie above the reference DTM. Simply subtracting them and computing the RMS value of the height differences does not yield an adequate accuracy measure for the MEOSS-DTM. In Figure 8, the image information for the DTM area is shown. Comparing Figures 7 and 8, the forests are clearly visible in the difference DTM in the upper part of Figure 7.

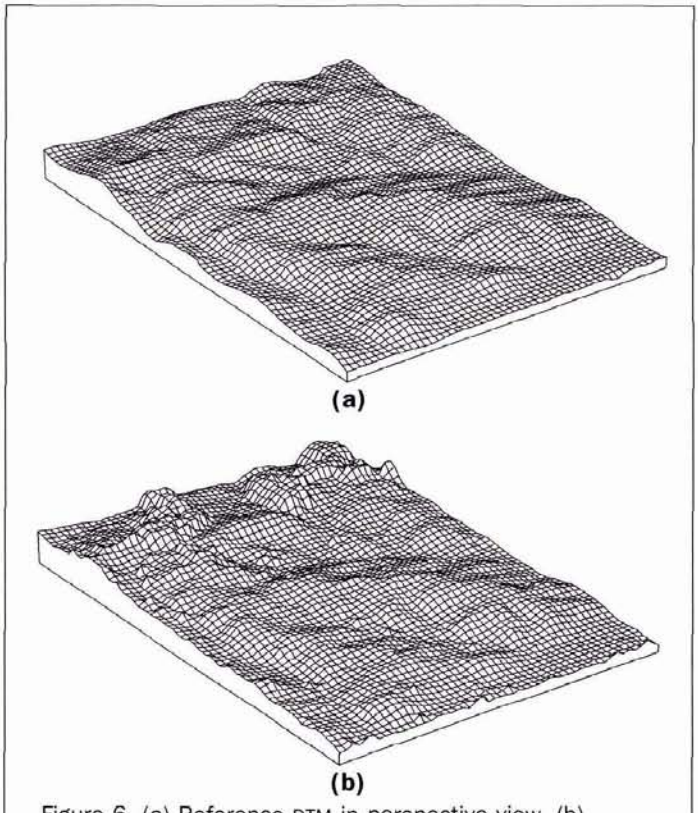

Figure 6. (a) Reference DTM in perspective view. (b) MEOSS-DTM in perspective view.

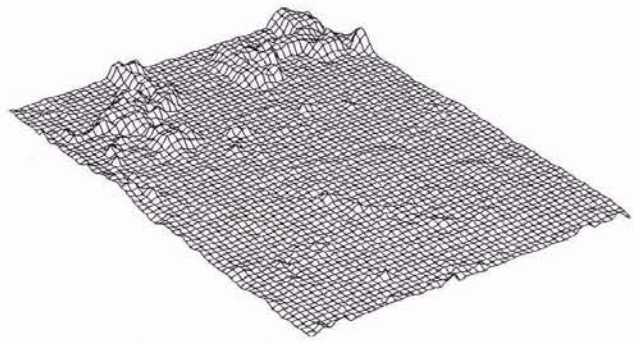

Figure 7. Difference DTM between MEOSS-DTM and reference DTM in perspective view.

Figure 8. Image information for the DTM area (part of the MEOSS WE nadir-looking image strip).

Conclusions

The presented material constitutes the results of the digital photogrammetric evaluation of airborne MEOSS imagery. Within the overlap of two crossing flight paths, an empirical accuracy of about 1 m or 0.5 pixel in X and Y, respectively, and 2.0 m or 1 pixel in height was achieved as verified by independent check points. Furthermore, it was shown that the simultaneous adjustment of two flight paths does not require navigation data, whereas the adjustment of a single flight path does. This corresponds to results from simulation studies (Ebner *et al.*, 1991; Ebner *et al.*, 1992). The selection of the weights for considering the different groups of observations in the adjustment still needs to be optimized. From the corresponding points, a DTM with similar accuracy was generated describing the visible Earth surface. The comparison with an interactively measured "bare Earth" reference DTM revealed differences mainly in forest areas.

The usefulness of the applied concept has thus been proven. Further research will be directed to a refinement of the matching algorithm in order to match more than two images simultaneously, and to simultaneous processing of whole image blocks rather than to one or two flight paths only. Furthermore, the experience gained in this study will be of great help for the processing of the MOMS-02/D2 and the Mars 94-HRSC/WAOSS imagery.

Acknowledgments

We wish to thank the German Aerospace Research Establishment (DLR) and especially Manfred Lehner for providing us with the MEOSS imagery; the Bayerisches Landesvermessungsamt for kindly making available the control data; Hermann Rentsch, Christian Wiedemann, Friederike Möβbauer, and Christian Piechulleck for their support; and last but not least Heinrich Ebner, Head of the Chair for Photogrammetry and Remote Sensing at the Technical University Munich, for giving us guidance throughout the study. Without the help of all of them, the study could not have been conducted. During the ISPRS Commission IV Symposium in Athens, Georgia, in 1994, this paper received the best poster award of Working Group IV/2.

References

Ackermann, F., J. Bodechtel, F. Lanzl, D. Meissner, and P. Seige, 1989. MOMS-02 ein multispektrales Stereo Bildaufnahmesystem für die zweite deutsche Spacelab Mission D2, *Geo-Informationssystem (GIS)*, 2(3):5-11.

Albertz, J., F. Scholten, H. Ebner, C. Heipke, and G. Neukum, 1993. The camera experiments HRSC and WAOSS on the Mars 94/96 missions, *Geo-Informationssysteme (GIS)*, 6(4):11-16.

Ebner, H., W. Reinhardt, and R. Höβler, 1988. Generation, management, and utilization of high fidelity digital terrain models, *International Archives of Photogrammetry and Remote Sensing*, 27(B11,III):556-566.

Ebner, H., W. Kornus, G. Strunz, O. Hofmann, and F. Müller, 1991. A simulation study on point determination using MOMS-02/D2 imagery, *Photogrammetric Engineering & Remote Sensing*, 57(10):1315-1320.

Ebner, H., W. Kornus, and T. Ohlhof, 1992. A simulation study on point determination for the MOMS-02/D2 space project using an extended functional model, *International Archives of Photogrammetry and Remote Sensing*, 29(B4,IV):458-464.

Förstner, W., 1982. On the geometric precision of digital correlation, *International Archives of Photogrammetry and Remote Sensing*, 24(3):176-189.

Heipke, C., 1990. *Integration von digitaler Bildzuordnung, Punktbestimmung, Oberflächenrekonstruktion und Orthoprojektion in der digitalen Photogrammetrie*, Deutsche Geodätische Kommission C-366.

Heipke, C., and W. Kornus, 1991. Nonsemantic photogrammetric processing of digital imagery — the example of SPOT stereo scenes, *Digital Photogrammetric Systems* (H. Ebner, D. Fritsch, and C. Heipke, editors), Wichmann, Karlsruhe, pp. 86-102.

Heipke, C., W. Kornus, R. Gill, and M. Lehner, 1990. Mapping technology based on 3-line-camera imagery, *International Archives of Photogrammetry and Remote Sensing*, 28(4):314-323.

Heipke, C., P. Saisi, and M. Stephani, 1994. Art inventarisation and preservation by digital photogrammetry, *International Archives of Photogrammetry and Remote Sensing*, 30(5):171-177.

Hofmann, O., 1986. Dynamische Photogrammetrie, *Bildmessung und Luftbildwesen*, 54(3):105-121.

Hofmann, O., A. Kaltenegger, and F. Müller, 1993. Das flugzeuggestützte, digitale Dreizeilenaufnahme- und Auswertesystem DPA -erste Erprobungsergebnisse, *Photogrammetric Week '93* (D. Fritsch and D. Hobbie, editors), Wichmann, Karlsruhe, pp. 97-107.

Hofmann, O., P. Navé, and H. Ebner, 1982. DPS — A digital photogrammetric system for producing digital elevation models (DEM) and orthophotos by means of linear array scanner imagery, *International Archives of Photogrammetry and Remote Sensing*, 24(3):216-227.

Kornus, W., 1989. *Praktische Untersuchung zur Punktbestimmung mit Bilddaten digitaler Dreizeilenkameras*, Diploma Thesis, Chair for Photogrammetry and Remote Sensing, Technical University Munich.

Lanzl, F., 1986. The monocular electro-optical stereo scanner (MEOSS) satellite experiment, *International Archives of Photogrammetry and Remote Sensing*, 26(1):617-620.

Lehner, M., and R. Gill, 1989. Photogrammetric adjustment of triple stereoscopic Imagery of an airborne CCD Scanner, *Optical 3-D Measurements Techniques* (A. Grün and H. Kahmen, editors), Wichmann, Karlsruhe, pp. 123-132.

———, 1992. Semi-automatic derivation of digital elevation models from stereoscopic 3-line scanner data, *International Archives of Photogrammetry and Remote Sensing*, 29(B4):68-76.

Lehner, M., and W. Kornus, 1994. Intermediate status report on the stereoscopic evaluation of combined stereoscopic (along track) and multispectral data of the MOMS-02 sensor, *International Archives of Photogrammetry and Remote Sensing*, 30(4):441-448.

Müller, F., 1991. *Photogrammetrische Punktbestimmung mit Bilddaten digitaler Dreizeilenkameras*, Deutsche Geodätische Kommission C-372.

Neukum, G., and V. Tarnopolski, 1990. Planetary Mapping - the Mars cartographic data base and a cooperative *Geo-Informationssysteme (GIS)*, 3(2):20-29.

Oertel, D., R. Reulke, R. Sandau, M. Scheele, and T. Terzibaschian, 1992. A flexible digital wide-angle optoelectronic stereo scanner, *International Archives of Photogrammetry and Remote Sensing*, 29(B1):44-49.

Otto, G.P., and T.K.W. Chau, 1989. 'Region growing' algorithm for matching of terrain images, *Image and Vision Computing*, 7(2): 83-94.

Reulke, R., M. Scheele, and T. Terzibaschian, 1992. Optoelektronischer Weitwinkelscanner von Mars-94/96 in der Flugerprobung, *bild&ton*, 45(9/10):293-301.

(Received 21 July 1994; accepted 29 November 1994; revised 12 January 1995)